On-sun performance and stability of graphene nanofluids in concentrating direct absorption solar collectors

Miguel Sainz-Manas, Alexis Vossier, Roger Garcia, Cyril Caliot, Françoise Bataille, Gilles Flamant

Sustainable Energy Technologies and Assessments 83 (2025) 104605

Contents lists available at ScienceDirect

Sustainable Energy Technologies and Assessments

journal homepage: www.elsevier.com/locate/seta

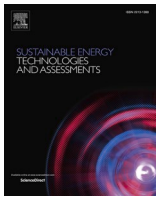

Original article

On-sun performance and stability of graphene nanofluids in concentrating direct absorption solar collectors

Miguel Sainz-Manas [a,b], Alexis Vossier [a], Roger Garcia [a], Cyril Caliot [c], Françoise Bataille [a,b], Gilles Flamant [a,*]

[a] Processes, Materials and Solar Energy Laboratory, PROMES – CNRS, 7 rue du Four Solaire, 66120 Odeillo, France
[b] UPVD, Rambla de la Thermodynamique, Tecnosud 66100 Perpignan, France
[c] LMAP, UPPA, CNRS, E2S, 1 allée du parc Montaury, 64600 Anglet, France

ARTICLE INFO

Keywords:
Solar thermal energy
Direct absorption solar collector (DASC)
Parabolic trough concentrator (PTC)
Thermal stability of graphene dispersion
Experimental study

ABSTRACT

The Performances of direct absorption solar collectors (DASC) are limited by the stability of the nanofluid's optical properties. This study investigates the performance and long-term stability of a graphene-based nanofluid under real on-sun operating conditions using an experimental parabolic trough pilot. The on-sun experiments were complemented with a detailed off-sun experimental evaluation of the nanofluid stability with temperature. Experimental results show that while the nanofluid optical properties remained stable over long periods (over two and a half months) and across varying temperatures (up to 80 °C) in a controlled environment, exposure to actual operational conditions in a parabolic trough collector working in closed loop caused significant degradation of optical properties, particularly due to pH changes due to corrosion in the collector hydraulic circuit. Despite this, overall photo-thermal conversion efficiencies of 62.3 ± 0.6 % and 74.3 ± 0.8 % were achieved with graphene concentrations of 0.2 and 0.3 g/L respectively, a substantial improvement over the 24.5 ± 0.5 % achieved using demineralized water. These findings highlight the critical role of material compatibility in hydraulic systems with graphene/water nanofluids to minimize corrosion, maintain particle stability and preserve collector performance in practical applications.

Introduction

Although transitioning towards a renewable electricity grid is essential for the energy transition, heat demand accounts for half of the final energy consumption worldwide [1]. In the industrial sector, heat represents 74 % of the total energy demand [2]. Therefore, decarbonizing the thermal power demand is crucial for mitigating climate change. For this purpose, no-concentrating and low-concentrating solar thermal collectors offer an economical alternative to conventional heat sources. Non-concentrating collectors generate heat below 120 °C for residential heating and cooling and low temperature industrial processes. Small to medium size concentrating solar thermal collectors can generate temperatures above 150 °C, a temperature range of great industrial significance due to its usefulness in a broad spectrum of industrial processes [3–6]. Another option towards generating high-temperature heat consists in coupling photovoltaic (PV) modules with high temperature heat pumps or other heating devices [7,8]. In the last decades, new concepts of thermal and hybrid PV-thermal collectors have motivated researchers for higher total conversion efficiencies. Among these new concepts, direct absorption solar collectors (DASC) attracted the attention of the scientific community [9].

Contrary to conventional solar thermal collectors, DASC use a semitransparent heat transfer fluid (HTF) to directly absorb the incident radiation within the fluid volume, eliminating the selective absorbing surface of conventional receivers. The optical absorption of conventional HTF, such as water or thermal oils, can be tuned by adding nanosized particles, leading to an increase in the efficiency of volumetric receivers (the particle dispersion within the host fluid being often referred to as *nanofluid*). The efficiency of non-concentrating collectors with low particle volume fractions (< 0.1 vol%) has been shown to be similar to that of conventional planar collectors [10–14]. Concentrating DASC research has focused on parabolic trough (PTC) and linear Fresnel collectors (LFC) of small and medium size due to stability limitations of nanoparticle dispersions at high temperatures [15,16]. Using a CuO/oil nanofluid, Xu *et al.* [17] experimentally evaluated the efficiency of a parabolic trough direct absorption solar collector (PT-DASC), finding a total efficiency decrease from ≈ 62 % to ≈ 40 % when the inlet

* Corresponding author at: Processes, Materials and Solar Energy laboratory, PROMES – CNRS, 7 rue du Four Solaire, 66120 Odeillo, France.
E-mail address: Gilles.Flamant@promes.cnrs.fr (G. Flamant).

https://doi.org/10.1016/j.seta.2025.104605
Received 13 May 2025; Received in revised form 30 August 2025; Accepted 21 September 2025

Nomenclature

A	Aperture area – m^2
C_p	Specific heat capacity – $J.kg^{-1}.K^{-1}$
E	Incident energy – kWh
G	Incident radiation – $W.m^{-2}$
$I_{AM1.5D}$	Solar spectral irradiation – $W.m^{-2}.nm^{-1}$
$\dot{m}$	Mass flow rate – $kg.s^{-1}$
P	Heat power – W
t	Time – s
T	Temperature – $°C$
ΔT	Temperature difference ($T_{out} - T_{in}$) – K

Acronyms

BRDF	Bidirectional reflectance distribution function
CTM	Camera target method
CW	Carbon Waters
DASC	Direct absorption solar collector
DNI	Direct normal irradiance
DW	Demineralized water
HTF	Heat transfer fluid
NDASC	Nanofluid direct absorption solar collector
PTC	Parabolic trough collector
PT-DASC	Parabolic trough-direct absorption solar collector
RTD	Resistance temperature detector

Greek letter

α	Absorptivity
β	Extinction coefficient – m^{-1}
γ	Intercept factor
η	Efficiency
λ	Wavelength – nm
ρ	Reflectivity
τ	Transmissivity
τ_{d_r}	Directional transmissivity

Subscripts

0	Initial condition
amb	Ambient
an	Analytical
avg	Average
col	Collector
exp	Experimental
glass	Glass
in	Inlet
loss	Losses
out	Outlet
PT	Photo-thermal
ref	Reflector
tot	Total
u	Useful
work	Working

temperatures increases from 55 ℃ to 160 ℃ respectively. Menbari *et al.* [18] and Heyhat *et al.* [19] found PT-DASC efficiencies between 49–65 % using a CuO/water HTF with particle concentrations between 0.01–0.1 vol%. When combining CuO and Al_2O_3 nanoparticles, purely water-based dispersions offer higher efficiencies than ethylene glycol–water mixtures when tested in PT-DASC [20,21].

Among the different nanoparticle families, carbon-based nanoparticles offer higher DASC performances, thanks to their outstanding optical and thermo-physical properties as well as their long term stability [10,11,22–29]. Among carbon nanoparticles, graphene has attracted significant attention owing to its original optical properties, intrinsic to its 2D morphology. Graphene nanoplatelets have a high surface-to-volume ratio, enabling higher absorption at similar volume fractions compared to other nanoparticle dispersions. Several studies have tested experimentally graphene-oxide [30–32] and graphene [33–35] nanoplatelets in planar collectors. Sattar *et al.* [32] compared the performance of various particle dispersions and found the best results with graphene-oxide nanoparticles. Vakili *et al.* [34] measured the performance of a flat plate DASC with graphene nanoplatelets dispersed in water, showing an increase on the collector efficiency with the nanoparticle concentration due to an increase of the nanofluid absorptivity. Wang *et al.* [27] studied the performance of a graphene/oil nanofluid with a solar simulator that concentrates the incident radiation towards a tubular receiver. The authors observed higher performances of the graphene/oil dispersion compared with CuO and graphite oil dispersions. To the authors' knowledge, no experimental study has been published evaluating the on-sun performance of a graphene aqueous dispersion working in a parabolic trough NDASC.

The stability of nanofluids is a key parameter for their applications in either drug delivery, heat transfer fluids, lubrication and other [36,37]. A nanofluid is considered unstable when presenting pronounced sedimentation and/or agglomeration of nanoparticles affecting its optical or thermo-physical properties. Nanoparticle agglomeration entails an increase of size which results in a degradation of the radiation absorption of the nanofluid. Simultaneously, particle agglomeration can result in sedimentation, leading to a concentration gradient along the fluid and particle deposition at the bottom of the recipient. Key parameters affecting the nanofluid stability and the main mechanisms to reduce its impact are exhaustively reviewed in Chakraborty *et al.* [36], Mukherjee *et al.* [37] and Mehta *et al.* [38] articles. Among these, the pH and the working temperature of the fluid are key parameters. The pH of the dispersion has a direct impact on the repulsive forces between the particles, which isoelectric point (molecules carry a net charge of zero) must be avoided. Higher working temperature increase Brownian motion, which causes agglomeration and sedimentation of the particles.

A considerable body of research has been dedicated to the study of the stability of nanoparticles at ambient temperature (around 25 °C). Nevertheless, research into the stability of these compounds at temperatures compatible with concentrated solar flux applications remains limited. Chang *et al.* [39] observed agglomeration and loss of particle stability of CuO particles dispersed in water at 40 °C, with a higher particle agglomeration as the temperature increased. Similar results were obtained by Tavares *et al.* [40] for a Cu-Ethylene glycol nanofluid working at temperatures up to 85 °C (boiling point). Their study suggests that the particle agglomeration is due to the intensification of the Brownian motion, and can be mitigated using an ultrasound bath, allowing a re-dispersion of the agglomerated particles. In the case of graphene, Chen *et al.* [30] observed a decrease in the zeta potential of graphene and graphene oxide water dispersions with fluid temperature increasing from 30 °C to 70 °C, leading to stability degradation and a decrease of the optical properties of the nanofluids. The authors however do not explicitly explain the mechanism responsible of the zeta potential decreases with temperature.

Various graphene oxide dispersions, both alone and combined with carbon nanotubes, exhibited an increase in the extinction coefficient after irradiation and heating up to 80 °C using a solar simulator [41,42]. This phenomenon was attributed to the photoreduction of some graphene-oxide particles under illumination, leading to a color change in the samples. While the samples appeared stable to the naked eye, the influence of temperature on their optical properties could not be exhibited, as it was hidden by particle photoreduction. A key limitation of these combined experimental protocols is the difficulty in

discriminating between the independent effects of solar radiation and temperature. A more detailed experimental design isolating the two factors is essential for accurately assessing the practical use of such fluids.

The particle stability at elevated temperatures under controlled environments is a crucial step towards the use of nanofluids in concentrating DASC. However, real operating conditions, such as concentrated radiation, pH fluctuations or other environmental factors, can significantly accelerate particle stability degradation [36]. Isolating these external factors to identify those responsible for the accelerated degradation of the nanofluid is often challenging. Moreover, there is a lack of studies addressing the stability of graphene-water nanofluids in a representative on-sun environment. This work aims to study the evolution of the optical properties of graphene-water nanofluids under operating conditions representative of DASC and to relate these changes to the thermal performance of the collector. The novelty of this work lies in combining on-sun and off-sun experiments to isolate the specific effects of temperature and other external factors on nanofluid degradation.

To this end, a small-scale on-sun PT-DASC pilot was built and instrumented to monitor collector optical and thermal efficiencies using several concentrations of graphene nanoparticles dispersed in water. This approach was complemented by off-sun experiments evaluating the nanofluid stability under controlled temperature (up to 80 °C) and environmental conditions over time periods of up to 2.5 months. This dual approach enables the isolation of nanofluid degradation effects driven by elevated temperatures from those caused by the integration into DASC concentrators (e.g., exposure to concentrated solar flux or fluid circulation).

First, the temporal evolution of the nanofluid's optical properties was examined at ambient temperature and across different graphene concentrations to assess particle stability. Next, the nanofluids were exposed to higher operating temperatures to explore the temperature-dependence of the particle stability. Finally, on-sun experimental campaigns under concentrated radiation were conducted on a small-scale PT-DASC pilot to investigate the influence of operating conditions on both particle stability and collector efficiency. The study concludes with a detailed discussion of key parameters significantly affecting system performance and provides recommendations to support the development of graphene nanofluid-based DASC.

Methodology

The aqueous dispersion used in this study, ref. CW-GLB02A1 (supplied by Carbon-Waters®), is composed of hydroxylated graphene particles, which provides a electrostatic repulsion between single layer graphene sheets [43–45]. The pH of the initial nanofluid is found between 7.5 and 8.5, with a zeta potential of −45 mV [44]. The authors of the latter paper observed an increase of the zeta potential with the acidification of the fluid, leading to an imminent unstable dispersion for pH below 4.

Particle stability under controlled environment

Samples with graphene concentration of 0.1 g/L, 0.2 g/L, and 0.3 g/L were obtained by diluting the initial Carbon Waters® 1 g/L solution with demineralized water (Table 1, together with Fig. S1 in the supplementary information). These concentrations were chosen based on their optical absorption properties, previously analyzed in our earlier work [46], to ensure sufficient absorption of incident solar radiation within the receiver of the studied parabolic-trough pilot (extinction coefficients of 36.5 m^{-1}, 62.3 m^{-1} and 87.7 m^{-1} for 0.1 g/L, 0.2 g/L and 0.3 g/L respectively). A spectrophotometer was used to measure the directional transmissivity (τ_{d_τ}) of these dilutions (Table S1 in the supplementary information).

Table 1
Samples used in the optical and stability characterization.

Samples	Graphene concentration	Uncertainty
DW	Demineralized water	–
CW-0.1	0.1 g/L *(0.01 wt%)*	± 0.021 g/L
CW-0.2	0.2 g/L *(0.02 wt%)*	± 0.021 g/L
CW-0.3	0.3 g/L *(0.03 wt%)*	± 0.021 g/L

In our previous work, the optical properties of the graphene aqueous dispersion were analyzed experimentally and numerically, concluding that scattering has a negligible effect on the total light extinction [46]. The measured τ_{d_τ} allows the calculation of the extinction coefficient (β) with the Beer-Lambert's law (Fig. S2 in the supplementary information).

Assessing the temporal evolution of the nanofluid optical properties is a convenient tool to quantify agglomeration or sedimentation of particles, and thus its stability [47,48]. Firstly, in order to facilitate a deeper comprehension of the origins of the degradations in optical properties likely to be encountered under real operating conditions, the temporal evolution of the optical properties of nanofluids under controlled environment for varying periods of time is characterized. The aim here is to expose several nanofluid samples to different thermal histories, by imposing a thermal stress on them for a more or less long period of time, then keeping them at room temperature. The optical properties of the nanofluids are characterized at regular intervals in order to quantify the extent of degradation during ageing.

First, nanofluid samples were maintained at ambient temperature over 1800 h and the τ_{d_τ} variation with time was measured (noted CW1 in Fig. S3). Two samples with 0.1 and 0.2 g/L particle concentrations are evaluated within this case.

Secondly, nanofluid samples have been placed in a water bath at 80 °C for different time periods and the evolution of their optical properties was measured. All experiments at 80 °C were organized in four different cases, noted CW2 to CW5, each one composed of 0.1 and 0.2 g/L samples, which protocols are detailed in Fig. S3. The tendencies found for these two dilutions are assumed similar for other particle concentrations.

Experimental set-up

Parabolic trough collector

A 2 m long and 0.96 m wide (aperture) parabolic trough DASC has been designed and built at the PROMES laboratory (France) (Fig. 1). The concentrator is placed on a 2-axis solar tracking structure coupled with two electric linear actuators. A microcontroller board is used to manage the linear actuators and automatically control the position of the concentrator. High specular reflectance thin aluminum sheets are attached to marine plywood ribs to obtain the parabolic profile of the concentrator. The Almeco® VWR193 aluminum reflector, 0.4 mm thickness, was found to provide a high specular reflectance in the whole sun spectra (further information on the pilot design and reflectivity measurements is given in the supplementary information).

The receiver is a double glass evacuated tube placed at the focal line of the concentrator (1 mbar pressure at the annulus). The selected nanofluid flows inside the internal tube (33.6 mm id) at ambient pressure (1 bar) and absorbs the concentrated radiation (Fig. 1). Borosilicate glass has been chosen due to its thermal strength and transparency in the visible and near-infrared range. A Warson Marlow peristaltic pump is positioned before the inlet of the receiver (Fig. 1). The fluid flow rate ranges between 60 and 120 L/h, resulting in average fluid velocities from 0.018 to 0.038 m/s corresponding to a Reynolds number below 2300 (laminar flow). The fluid temperature at the inlet and outlet of the receiver tube is measured with PT100 platinum resistance temperature detectors (RTD). After the outlet temperature sensor, the fluid is guided towards a cooling radiator.

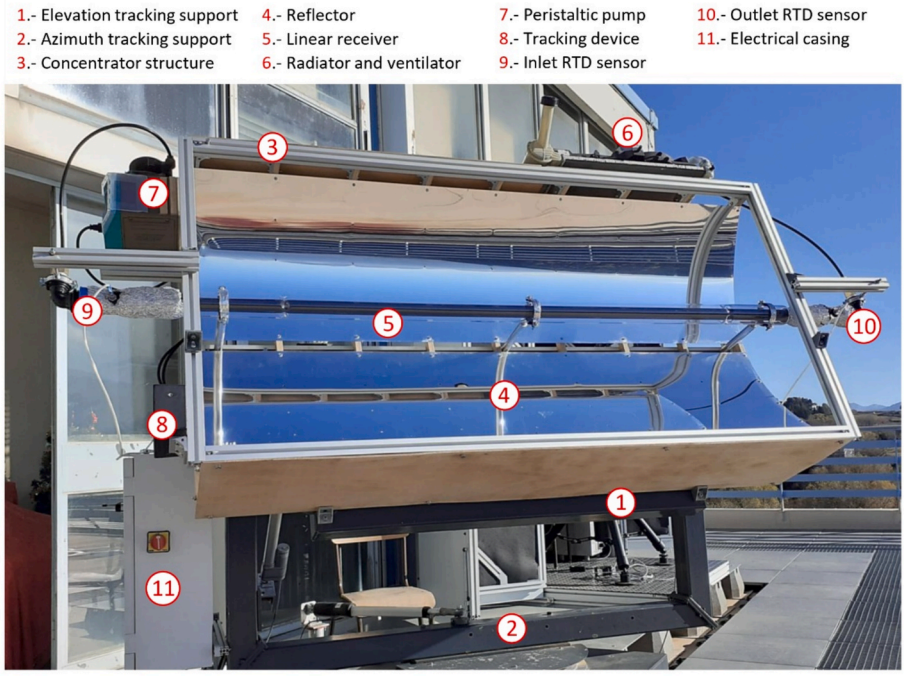

Fig. 1. Picture of the PT-DASC experimental setup built at the PROMES laboratory.

Performance metrics

The fluid temperature increase (ΔT) throughout the receiver is defined as the difference between the outlet and inlet HTF temperature measured with the RTD sensors, T_{out} and T_{in} respectively. The useful power (P_u) gained by the HTF throughout the collector is defined as:

$$P_u = \dot{m} C_p \Delta T \tag{1}$$

where $\dot{m}$ is the mass flow rate, and C_p is the isobaric specific heat of the HTF. The total efficiency of the PT-DASC (η_{tot}), is defined as the ratio of P_u to the incident solar power at the concentrator aperture:

$$\eta_{tot} = \frac{P_u}{A_{col} G_0} \tag{2}$$

where A_{col} is the concentrator aperture area, and G_0 the measured DNI.

The system heat losses were characterized at night in order to minimize the probability of absorption of parasitic photons, which could bias the rigorous assessment of heat losses. The influence of the graphene particle concentration on the thermo-physical properties of the HTF were assessed, revealing negligible impact at low particle concentrations (see Annex 9). Consequently, demineralized water was used as HTF for the thermal loss experiments. A JULABO Cryo-Compact Circulator CF30 (ref. 9400330.04) was used to regulate and maintain the temperature of the fluid entering the receiver. By measuring the temperature difference between T_{in} and T_{out} the power heat losses (P_{loss}) throughout the receiver can be calculated with the following equation:

$$P_{loss} = \dot{m}\, C_p\, (T_{in} - T_{out}) \tag{3}$$

Heat losses from the fluid to the environment depend on the difference between the HTF temperature and the ambient temperature, T_{amb}. Higher differences between these temperatures result in higher heat losses. The measured heat losses are presented in Annex 10 of the supplementary information as a function of $T_{avg} - T_{amb}$, with $T_{avg} = (T_{in} + T_{out})/2$.

The photo-thermal efficiency, η_{PT}, is defined as the ratio of the power absorbed by the fluid (P_{PT}) to the incident power at the concentrator aperture. Considering the above-mentioned definitions, the power balance of the HTF can be expressed as:$P_u = P_{PT} - P_{loss}$. Therefore, the experimental photo-thermal efficiency, $\eta_{PT,exp}$, of the collector can be obtained with the following equation:

$$\eta_{PT,exp} = \frac{P_u + P_{loss}}{A_{col} G_0} \tag{4}$$

Analytically, the photo-thermal efficiency, $\eta_{PT,an.}$, is calculated based on the specific optical properties of each of the components of the collector:

$$\eta_{PT,an} = \rho_{ref} \tau_{glass} \alpha_{HTF} \gamma \tag{5}$$

where ρ_{ref} is the mirror directional reflectivity, τ_{glass} the transmissivity of the glass tube, α_{HTF} the HTF absorptivity, and γ the intercept factor of the receiver (values given in Table 2). α_{HTF} is calculated with the measured HTF extinction coefficient β considering the inner diameter of the receiver, 33.6 mm. The γ is considered equal to 1 as a result of the qualitative data using the Camera Target Method detailed in the supplementary information. All spectral properties are integrated over the AM1.5D solar spectrum between 250 and 2500 nm from ASTM G173-03 [49], similarly as in equation S1 in the annexes.

The temporal evolution of the optical properties of the HTF under real operating conditions is quantified by measuring τ_{d_τ} of the samples. From τ_{d_τ}, β is obtained with the Beer-Lambert's law. Graphene absorption properties essentially contribute below 1350 nm, as water absorption dominates significantly at longer wavelengths. For this reason, β is integrated over the AM1.5D solar spectrum between 250 and 1350 nm from ASTM G173-03 [49]. Instead of evaluating the evolution of β with time, it is evaluated as a function of the incident energy to the collector,

Table 2
Parameters used for the analytical evaluation of the photo-thermal efficiency of the collector.

Parameter	Value	Details
ρ_{ref}	87.94 ± 0.13 %	Almeco VWR193 (sup. info.)
τ_{glass}	97 %	Borosilicate glass from ref. [50]
α_{water}	28.72 ± 0.15 %	Water
$\alpha_{CW-0.1}$	70.66 ± 0.07 %	0.1 g/L nanofluid
$\alpha_{CW-0.2}$	87.69 ± 0.03 %	0.2 g/L nanofluid
$\alpha_{CW-0.3}$	94.75 ± 0.02 %	0.3 g/L nanofluid
γ	1	from CTM qualitative analysis

E_0, expressed as: $E_0 = G_0 A_{col} t_{work}$, with t_{work} the working time of the HTF under solar concentration.

Results

Nanofluid stability under controlled environment

The optical properties of CW1 samples maintained at ambient temperature for over 1800 h are plotted in Fig. 2. Both nanoparticle concentrations, 0.1 and 0.2 g/L, show similar transmissivity spectra independent of the measurement time. The small deviations between curves are within the spectrophotometer measurement uncertainty (see Table S1 in the annexes). The long-term stability can be granted to all samples at ambient temperature.

The influence of temperature on the nanofluid transmissivity at 600 nm is represented in Fig. 3 for the four cases under 80 °C water bath illustrated in Fig. S3, CW2 to CW5. It must be noted that similar tendencies are found for other wavelengths in the whole spectrum. The variation of τ_{d_τ} with time is shown to be negligible, less than 2 %, for all cases and particle concentrations, and within the measurement uncertainty. An unexplained increase in τ_{d_τ} of fluid *CW3-0.1* is observed at the second measurement point, possibly related to measurement error as subsequent measurements do not confirm the increase observed at this point.

The presented results concur with the reported dispersion stability by the supplier. As no surfactant is used for the graphene dispersion, the temperature increase does not affect its degradation, a point which can be a particularly problematic issue for other carbon-based nanofluids [10]. Nevertheless, the intensification of the Brownian motion with temperature could induce instability for the graphene dispersion. Previous figures prove however a long-term stability of all samples even at temperatures close to the boiling point of the base fluid. To conclude, no agglomeration nor sedimentation are expected when using these nanofluids in the PT-DASC experimental pilot.

Experimental results under real operating conditions

Performance of the concentrating NDASC pilot

The experimental characterization of the DASC concentrator is carried out under real sunlight conditions and is therefore subject to significant variations in the solar resource. The HTF is not pre-heated or cooled before entering the receiver, therefore T_{in} is close to ambient temperature, between 15 and 25 °C. Further information of the protocol used in the measurement campaigns can be found in Annex 11.

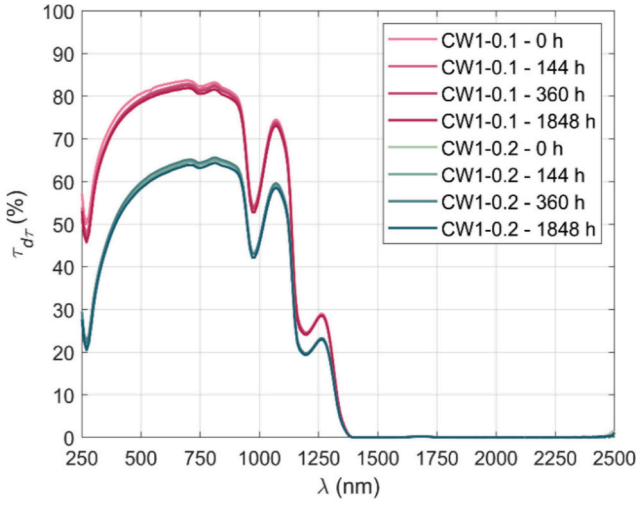

Fig. 2. Evolution of the τ_{d_τ} spectra of two different graphene dilutions at ambient temperature.

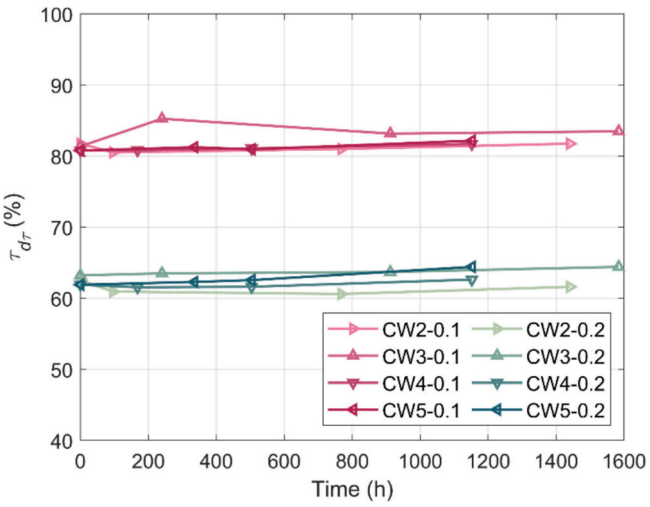

Fig. 3. τ_{d_τ} Evolution with time at 600 nm for cases CW2 to CW5 maintained under 80 °C water bath for 0.1 g/L (red) and 0.2 g/L (green). Each marker corresponds to a measurement campaign. (For interpretation of the references to colour in this figure legend, the reader is referred to the web version of this article.)

Fig. 4a shows the ΔT throughout the receiver for different flow rates and three different HTFs: water, and graphene dispersions of 0.2 g/L (CW-M−0.2) and 0.3 g/L (CW-M−0.3). All experiments have been repeated threefold to assure repeatability of the results. As expected, for all three HTF used, ΔT decreases with the flow rate, resulting of shorter times of the HTF under concentration through the receiver. When graphene nanoparticles are added to water, a significant increase in ΔT is obtained. CW-M−0.3 showed higher absorptivity than CW-M−0.2, which results in a higher temperature increase. At 120 L/h, both graphene dispersions show similar average ΔT, which is attributed to different average G_0 available at the moment of the experiments, ~ 1050 W/m^2 and ~900 W/m^2 for CW-M−0.2 and CW-M−0.3 respectively.

The total efficiency of the PT-DASC (η_{tot}) for each HTF studied is calculated with the average incident solar irradiance G_0 during the steady state regime (Fig. 4.**b**). As can be observed, η_{tot} is nearly constant and independent of the fluid flow rate for the three tested HTF at flow rate larger than 60 L/h. This behavior is related to the low temperature difference between the bulk fluid and the environment, which entails very low heat losses along the receiver. Consequently, η_{tot} is mainly attributed to the photo-thermal efficiency, η_{PT}, of the collector, which varies with the HTFs absorptivity but remains independent of the fluid flow rate. Nevertheless, heat losses may have a higher effect for higher temperature difference. The mean η_{tot} are 24.5 ± 0.5 %, 62.3 ± 0.6 %, and 74.3 ± 0.8 % for water, CW-M−0.2 and CW-M−0.3 respectively.

From equation (3), $\eta_{PT,exp}$ for each HTF tested can be calculated and compared to the expected $\eta_{PT,an}$ (Fig. 5). Increasing the particle concentration enhances the absorption capacity of the HTF, resulting in higher $\eta_{PT,exp}$ for the PT-DASC: 26.7 ± 0.5 %, 68.0 ± 0.6 % and 81.6 ± 0.8 % for water, CW-M−0.2 and CW-M−0.3 respectively. When compared with η_{tot}, the heat losses contribution can be deduced: 2.2 ± 0.7 %, 5.7 ± 0.8 %, and 7.3 ± 1.1 % for water, CW-M−0.2 and CW-M−0.3 respectively. Considering that the receiver tube is evacuated, these are primarily attributed to heat losses through the propylene connector at the outlet of the receiver tube, upstream of the temperature sensors. To minimize heat losses, this connector must be carefully insulated, particularly for experiments conducted at higher fluid temperatures.

The analytical calculations estimated accurately the $\eta_{PT,exp}$ for water and CW-M−0.3, but over estimated that of CW-M−0.2 by 2 to 10 %. Between the three cases, only the optical properties of the HTF changed,

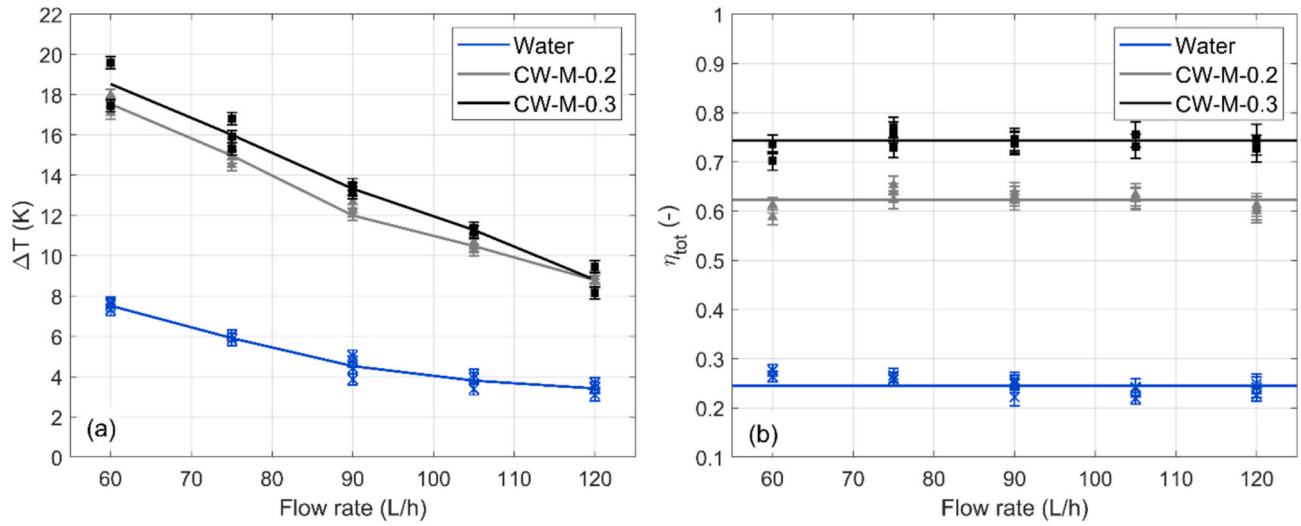

Fig. 4. Experimental results using different HTF showing (a) the temperature increase (ΔT) and (b) the total efficiency (η_{tot}). Each data points with error bars represent an experimental measurement while the solid lines represent the mean values for each flow rate.

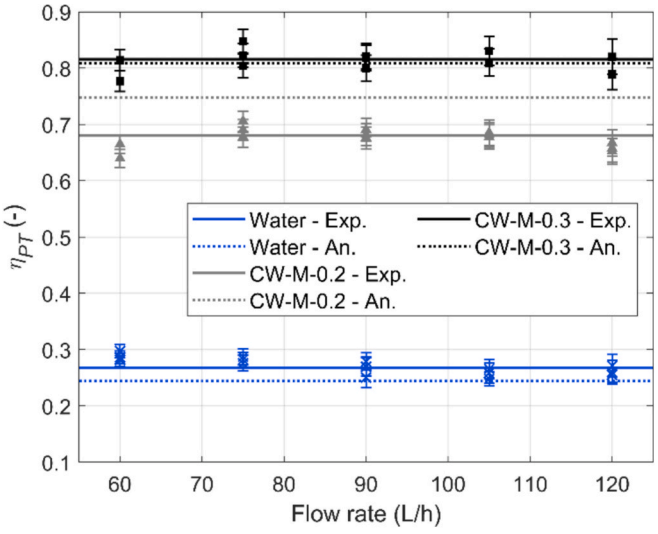

Fig. 5. η_{PT} Variation for different htf and flow rates. the points with error bars represent the experimental measurements, the solid lines represent the mean values of the experimental data points (eq.(4) and the dotted lines the analytical estimates for each HTF (Eq. (5).

thus suggesting a deterioration of the optical properties of the CW-M−0.2 nanofluid. To understand the highlighted difference between the analytical and experimental results, the temporal evolution of the optical properties of the nanofluid must be further studied.

Stability of the nanoparticles under real-operating conditions

Both the exposure to highly concentrated radiation and the circulation of the nanofluid within the DASC pilot is likely to result in increased degradation of the nanofluid, affecting the stability of the graphene dispersion and therefore its optical properties. To investigate the influence of the hydraulic circuit on particle stability, two experimental approaches were designed. First, the CW-M−0.2 nanofluid was tested using the PT-DASC pilot with corrosion-sensitive piping. Secondly, experiments were conducted using the CW-M−0.3 nanofluid but replacing the corrosion-sensitive connectors by non-corrosive materials, such as brass.

In the case of the CW-M−0.2 HTF, a significant decrease of β with E_0 was found after several days of experiments (Fig. 6**.a**). At the end of the experimental campaign, an 18 ± 1 % decrease of the initial extinction coefficient ($\beta_{0,CW-M-0.2} = 80.45 \pm 0.73$ m^{-1}) has been measured. This degradation explains the over-estimation of the photo-thermal efficiency with $\eta_{PT,an}$ in comparison with $\eta_{PT,exp}$ (see Fig. 5). The nanofluid optical properties degradation is not attributed to the fluid temperature, which did not exceed 40 °C, as previously tested nanofluids maintained their optical properties with time at 80 °C (see section 3). However, a significant decrease of the pH has been found for the CW-M−0.2 HTF during the experimental campaign (Fig. 6**.a**).

Several studies have reported a correlation between the pH of the dispersion and its stability [36–38,51,52]. In order to obtain high repulsion forces between the particles, the pH of the fluid must be significantly different from its isoelectric point, where molecules carry a net charge of zero. These forces between particles are quantified by the zeta potential. A particle suspension with a high absolute zeta potential is inherently stable (±30 mV), as high repulsion forces exist between the particles preventing agglomeration [36,51]. If the zeta potential decreases, in the ± 15 mV range, particles tend to agglomerate and thus the dispersion becomes unstable. The range of pH values consistent with high absolute zeta potentials is dependent on the base fluid and the nanoparticles used.

For the CW-M−0.2 nanofluid, the observed dispersion acidification from 7.5 to 6.5 pH led to the agglomeration of graphene particles and the formation of larger clusters. This increase in nanoparticle size reduced the number of individual optically active particles dispersed, thereby decreasing the extinction coefficient of the fluid. The strong sensitivity of nanofluid optical properties to changes in graphene size and shape was previously demonstrated by the authors [46], further supporting the direct relationship between fluid acidification, nanoparticle agglomeration and reduced extinction coefficient. The observed acidification is attributed to the corrosion of sensitive components of the hydraulic circuit (see photos of the steel connectors in the supplementary information), which may have contaminated the CW-M−0.2 fluid during experiments.

The CW-M−0.3 experimental campaign used non-corrosive components in the hydraulic circuit, expecting a lower impact of the hydraulic system on the pH, and thus on the HTF extinction coefficient, β. A decrease of 2 ± 1 % from the initial $\beta_{0,CW-M-0.3}$, 105.72 ± 0.91 m^{-1}, was measured after several experimental campaigns (Fig. 6**.b**). The pH stayed nearly constant with time for the CW-M−0.3 campaign, varying from 7.95 to 7.91, a significantly lower pH decrease compared to the CW-M−0.2 nanofluid. No corrosion of the hydraulic circuit was visible to the naked eye during this experimental campaign.

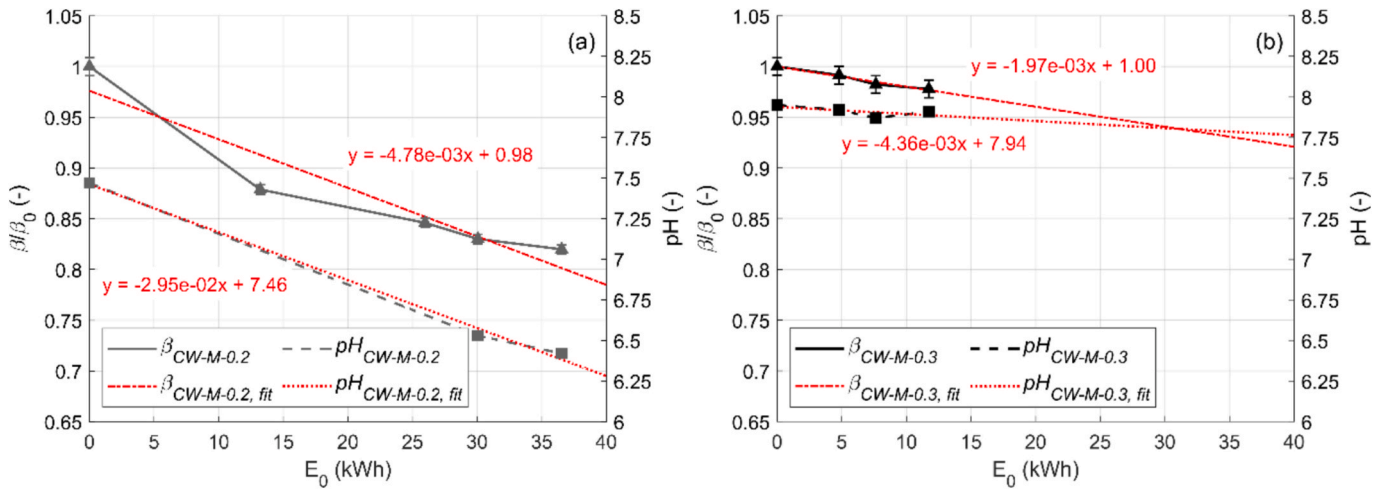

Fig. 6. Normalized β (solid line) and pH (dashed line) variation with E_0 for (a) CW-M−0.2 and (b) CW-M−0.3 as HTFs. The tendency lines of β (dash-dotted line) and pH (dotted line) for each HTF are plotted in red with their respective line equation. (For interpretation of the references to colour in this figure legend, the reader is referred to the web version of this article.)

The two above presented experimental approaches allowed the identification of sensitive components affecting the fluid hydrogen potential. Materials susceptible to corrosion, such as the steel used in the connectors, had a major influence on the pH of the nanofluid, which incited particle agglomeration. As a result, an important decrease of the nanofluid extinction coefficient was found after several experimental campaigns (Fig. 6**.a**). Using non-corrosive materials, such as brass, reduced the impact of the hydraulic circuit on the pH and the nanofluid extinction coefficient temporal evolution. As can be deduced from the slope of both β/β_0 fitted curves in Fig. 6, the optical properties of the HTF are degraded 2.4 times faster if corrosion-sensitive materials are used. While only graphene particles were studied here, corrosion is likely to affect the pH and optical properties of other carbon-based nanofluids, such as carbon nanotubes or carbon nanohorns dispersions.

Nevertheless, a slight decrease on the extinction coefficient was still found when corrosion resistant materials are used (Fig. 6**.b**). Two possible phenomena may explain these results: (1) residual corrosion within the hydraulic circuit, as the aluminum cooling radiator appears to remain susceptible to corrosion, or (2) a photochemical effect induced by concentrated radiation, leading to an increase in the hydrogen potential of the heat transfer fluid (HTF). In the nanofluid studied, the graphene sheets repulsive forces are the results of the OH^- ions at the particle surface. Photons incident to the dispersed particles might induce separation of the OH^- ions, thus influencing the hydrogen potential of the dispersion. To further evaluate this phenomenon, on-sun experiments must be conducted with a simpler hydraulic circuit avoiding parasite corrosion.

Corrosion of components has been listed among the main challenges for NDASC industrialization [10,11,53,54]. Both metal and metal-oxides induce higher corrosion in comparison with carbon-based nanofluids. In this study, however, corrosion has demonstrated to have a direct effect on the nanofluid optical properties. Preventing corrosion by the nanofluids is essential not only to avoid component degradation but also to preserve the stability of the nanofluids themselves. Materials in contact with the nanofluid should prioritize corrosion-resistant options such as brass, stainless steel, or surface-treated aluminum.

While chemically inert polymers such as PTFE or PEEK may offer corrosion resistance, their limited thermal stability at high operating temperatures makes them unsuitable for connectors at the receiver's outlet in future industrial thermal systems. Simplifying the hydraulic circuit by minimizing metal–nanofluid interfaces can also significantly reduce degradation risks. Additionally, incorporating a pH control system using a buffered solution may allow for direct management of chemical degradation, further preventing particle agglomeration and the progressive loss of nanofluid optical properties.

Although these design strategies may increase system installation costs in future industrial plants, they are expected to ensure greater nanofluid stability and system longevity, both of which are critical for large-scale deployment. Further work, including detailed techno-economic assessments, is encouraged to validate these design guidelines.

Conclusions and future work

The stability of nanofluids under real operating conditions and over long working periods is a prerequisite for the development of efficient, reliable and durable concentrating direct absorption solar collectors. A comprehensive understanding of the degradation mechanisms affecting the optical properties of nanofluids integrated into such systems is imperative. However, this is especially intricate due to the numerous factors that can lead to accelerated degradation of nanofluid stability (e.g., inherent instability of the fluid, temperature sensitivity, circulation in the system, exposure to concentrated solar flux, etc.…).

In this study, a methodology for identifying the causes of nanofluid degradation under real operating conditions is proposed, implemented and analyzed. The proposed method is rooted in the comparison of the degradation of nanofluids in two distinct environments: firstly, in a controlled environment where the nanofluid is subjected to ageing under controlled temperature conditions and for varying time-periods; and secondly, under real operating conditions, i.e., circulating under concentrated solar radiation in a DASC. This methodological approach facilitates the identification of the origin of nanofluid degradation, distinguishing between the intrinsic stability of the nanofluid and the degradation associated with the operation conditions within the DASC.

The proposed methodology enabled the confirmation of the good stability of the studied graphene aqueous dispersion. In a controlled environment at ambient temperature, the optical properties of all graphene dispersions remained constant for over two and a half months. Within the same environment, an increase in fluid temperature up to 80 °C, approaching the nanofluid boiling point, did not affect the stability of the particles. The optical properties of all the dilutions tested remained constant for over two months, independent of the thermal history imposed on it.

The performance of the DASC concentrator incorporating the graphene-based nanofluid was then determined, revealing that the total efficiency of the system increased significantly with nanoparticle

concentration, from 62.3 ± 0.6 % to 74.3 ± 0.8 % when using 0.2 and 0.3 g/L graphene dispersions. These efficiencies represent a substantial improvement over the 24.5 ± 0.5 % photo-thermal efficiency obtained with demineralized water. The fluid flow rate had a comparatively minor effect on the system efficiency, which is attributed to the low amplitude of the thermal losses given the characteristic temperatures reached in the system (which do not exceed 45 °C). At these working temperatures, conventional mature solar thermal technologies such as flat plate, evacuated tube or small-scale parabolic trough collectors attain collector efficiencies, between 60 to 75 % [55,56]. The measured graphene-based DASC collector efficiency reaches the upper limit of conventional existing solar collectors, demonstrating the feasibility and potential of the studied concept.

Finally, an accelerated degradation of the nanofluid's optical properties under real operating conditions was highlighted, probably caused by a rapid and significant drop in pH. The experimental protocol proposed here enables identifying the origin of the observed pH degradation with a good degree of certainty: in this case, it is the DASC hydraulic circuit that leads to accelerated corrosion and acidification of the fluid. This study emphasizes the crucial role of the DASC hydraulic system in preserving the optical properties and lifetime of nanofluids. It is evident that the incorporation of components sensitive to accelerated corrosion is likely to result in a rapid and substantial deterioration of the system's performance. While the observed correlation between pH and extinction coefficient is strong, a more detailed assessment of the underlying chemical mechanisms should be pursued in future studies (e.g., through zeta potential measurements, corrosion quantification, or spectroscopy). Isolating the many external factors that can influence nanofluid degradation requires comprehensive chemical analysis, a particularly challenging task when working with on-sun concentrating prototypes.

To develop concentrating direct absorption solar collectors (DASCs) that are operational at relevant temperatures (150–200 °C), it is essential to enhance our understanding of the behavior of nanofluids exposed to these characteristic temperatures, which remains beyond the scope of this study. This involves examining the impact of thermal losses through the receiver and assessing the benefits of adding low emissivity coatings to minimize radiative losses. Before considering the development of industrial-scale systems, it is necessary to deeply investigate the reported degradation mechanisms under a broader range of environmental and operational conditions. The degradation of the nanofluid optical properties associated with corrosion mechanisms can potentially increase in DASC working at elevated temperatures. In this context, the selection of non-corrosive materials such as brass, as shown in our study, can reduce pH variations and preserve nanofluid stability. However, detailed insights into the hydraulic system's design features (e.g., geometry, flow regimes, or protective linings) also remain beyond the scope of this study. Future research is therefore necessary, particularly under real and long-term operating conditions, to develop concrete recommendations on corrosion-resistant designs that can prevent particle agglomeration and sedimentation at high temperatures.

CRediT authorship contribution statement

Miguel Sainz-Manas: Writing – original draft, Software, Investigation, Formal analysis, Data curation, Conceptualization. **Alexis Vossier:** Writing – review & editing, Validation, Supervision, Methodology, Formal analysis, Conceptualization. **Roger Garcia:** Methodology, Investigation, Conceptualization. **Cyril Caliot:** Writing – review & editing, Supervision, Methodology, Formal analysis, Data curation, Conceptualization. **Françoise Bataille:** Writing – review & editing, Supervision, Project administration, Formal analysis, Data curation. **Gilles Flamant:** Writing – review & editing, Supervision, Resources, Project administration, Methodology, Funding acquisition, Conceptualization.

Declaration of competing interest

The authors declare that they have no known competing financial interests or personal relationships that could have appeared to influence the work reported in this paper.

Acknowledgements

The Perkin Elmer Lambda 950 spectrophotometer and SMS CASI® scatterometer belong to the PCM platform at the PROMES laboratory in Odeillo, and were operated by Christophe Escape. The direct normal irradiance (DNI) was measured with a Kipp & Zonen CH1 pyrheliometer, installed and operated by the Solar Installations and Associated Instruments (SISIA) department at the PROMES laboratory. The authors acknowledge Oliver Rebrioux, Michael Tessonneaud and Régis Rodriguez for their technical assistance during the experimental campaigns.

This work was supported by the French "Investments for the future" ("Investissements d'Avenir") and "France 2030" programs managed by the National Agency for Research (ANR) under contract ANR-10-LABX-22-01 (labex SOLSTICE) and ANR-22-PESP-0005 (SHIP4D project), respectively.

Appendix A. Supplementary data

Supplementary data to this article can be found online at https://doi.org/10.1016/j.seta.2025.104605

Data availability

Data will be made available on request.

References

[1] IRENA, Renewable power generation costs in 2022, International Renewable Energy Agency, Abu Dhabi, 2023.
[2] B. Epp, M. Oropeza, Solar Heat for Industry – Solar Payback, Solar Payback, 2017. https://www.solar-payback.com/wp-content/uploads/2017/07/Solar-Heat-for-Industry-Solar-Payback-April-2017.pdf.
[3] Kalogirou SA. Solar thermal collectors and applications. Prog Energy Combust Sci 2004;30:231–95. https://doi.org/10.1016/j.pecs.2004.02.001.
[4] A. Häberle, Concentrating solar technologies for industrial process heat and cooling, in: Concentrating Solar Power Technology, Elsevier, 2012: pp. 602–619. doi:10.1533/9780857096173.3.602.
[5] Sharma AK, Sharma C, Mullick SC, Kandpal TC. Solar industrial process heating: a review. Renew Sustain Energy Rev 2017;78:124–37. https://doi.org/10.1016/j.rser.2017.04.079.
[6] Farjana SH, Huda N, Mahmud MAP, Saidur R. Solar process heat in industrial systems – a global review. Renew Sustain Energy Rev 2018;82:2270–86. https://doi.org/10.1016/j.rser.2017.08.065.
[7] Jiang J, Hu B, Wang RZ, Deng N, Cao F, Wang C-C. A review and perspective on industry high-temperature heat pumps. Renew Sustain Energy Rev 2022;161:112106. https://doi.org/10.1016/j.rser.2022.112106.
[8] Arpagaus C, Bless F, Uhlmann M, Schiffmann J, Bertsch SS. High temperature heat pumps: Market overview, state of the art, research status, refrigerants, and application potentials. Energy 2018;152:985–1010. https://doi.org/10.1016/j.energy.2018.03.166.
[9] Tyagi H, Phelan P, Prasher R. Predicted efficiency of a low-temperature nanofluid-based direct absorption solar collector. J Sol Energy Eng 2009;131. https://doi.org/10.1115/1.3197562.
[10] Trong Tam N, Viet Phuong N, Hong Khoi P, Ngoc Minh P, Afrand M, Van Trinh P, et al. Carbon nanomaterial-based nanofluids for direct thermal solar absorption. Nanomaterials 2020;10:1199. https://doi.org/10.3390/nano10061199.
[11] Sainz-Mañas M, Bataille F, Caliot C, Vossier A, Flamant G. Direct absorption nanofluid-based solar collectors for low and medium temperatures. A review, Energy 2022;260:124916. https://doi.org/10.1016/j.energy.2022.124916.
[12] Chamsa-ard W, Brundavanam S, Fung CC, Fawcett D, Poinern G. Nanofluid types, their synthesis, properties and incorporation in direct solar thermal collectors: a review. Nanomaterials 2017;7:131. https://doi.org/10.3390/nano7060131.
[13] Kumar S, Chander N, Gupta VK, Kukreja R. Progress, challenges and future prospects of plasmonic nanofluid based direct absorption solar collectors – a state-of-the-art review. Sol Energy 2021;227:365–425. https://doi.org/10.1016/j.solener.2021.09.008.
[14] Karami M, Bozorgi M, Delfani S. Effect of design and operating parameters on thermal performance of low-temperature direct absorption solar collectors: a review. J Therm Anal Calorim 2021;146:993–1013. https://doi.org/10.1007/s10973-020-10043-z.

[15] Fu B, Zhang J, Chen H, Guo H, Song C, Shang W, et al. Optical nanofluids for direct absorption-based solar-thermal energy harvesting at medium-to-high temperatures. Curr Opin Chem Eng 2019;25:51–6. https://doi.org/10.1016/j.coche.2019.07.002.
[16] Rasih RA, Sidik NAC, Samion S. Recent progress on concentrating direct absorption solar collector using nanofluids: a review. J Therm Anal Calorim 2019;137:903–22. https://doi.org/10.1007/s10973-018-7964-6.
[17] Xu G, Chen W, Deng S, Zhang X, Zhao S. Performance evaluation of a nanofluid-based direct absorption solar collector with parabolic trough concentrator. Nanomaterials 2015;5:2131–47. https://doi.org/10.3390/nano5042131.
[18] Menbari A, Alemrajabi AA, Rezaei A. Heat transfer analysis and the effect of CuO/Water nanofluid on direct absorption concentrating solar collector. Appl Therm Eng 2016;104:176–83. https://doi.org/10.1016/j.applthermaleng.2016.05.064.
[19] Heyhat MM, Valizade M, Abdolahzade Sh, Maerefat M. Thermal efficiency enhancement of direct absorption parabolic trough solar collector (DAPTSC) by using nanofluid and metal foam. Energy 2020;192:116662. https://doi.org/10.1016/j.energy.2019.116662.
[20] Menbari A, Alemrajabi AA, Rezaei A. Experimental investigation of thermal performance for direct absorption solar parabolic trough collector (DASPTC) based on binary nanofluids. Exp Therm Fluid Sci 2017;80:218–27. https://doi.org/10.1016/j.expthermflusci.2016.08.023.
[21] Khalil A, Amjad M, Noor F, Hussain A, Nawaz S, Filho EPB, et al. Performance analysis of direct absorption-based parabolic trough solar collector using hybrid nanofluids. J Braz Soc Mech Sci Eng 2020;42:573. https://doi.org/10.1007/s40430-020-02654-2.
[22] Kasaeian A, Daneshazarian R, Rezaei R, Pourfayaz F, Kasaeian G. Experimental investigation on the thermal behavior of nanofluid direct absorption in a trough collector. J Clean Prod 2017;158:276–84. https://doi.org/10.1016/j.jclepro.2017.04.131.
[23] Bortolato M, Dugaria S, Agresti F, Barison S, Fedele L, Sani E, et al. Investigation of a single wall carbon nanohorn-based nanofluid in a full-scale direct absorption parabolic trough solar collector. Energ Conver Manage 2017;150:693–703. https://doi.org/10.1016/j.enconman.2017.08.044.
[24] Tafarroj MM, Daneshazarian R, Kasaeian A. CFD modeling and predicting the performance of direct absorption of nanofluids in trough collector. Appl Therm Eng 2019;148:256–69. https://doi.org/10.1016/j.applthermaleng.2018.11.020.
[25] T. Otanicar, R.A. Taylor, P.E. Phelan, R. Prasher, Impact of Size and Scattering Mode on the Optimal Solar Absorbing Nanofluid, in: ASME 2009 3rd International Conference on Energy Sustainability, Volume 1, ASMEDC, San Francisco, California, USA, 2009: pp. 791–796. doi:10.1115/ES2009-90066.
[26] Luo Z, Wang C, Wei W, Xiao G, Ni M. Performance improvement of a nanofluid solar collector based on direct absorption collection (DAC) concepts. Int J Heat Mass Transf 2014;75:262–71. https://doi.org/10.1016/j.ijheatmasstransfer.2014.03.072.
[27] Wang N, Xu G, Li S, Zhang X. Thermal properties and solar collection characteristics of oil-based nanofluids with low graphene concentration. Energy Procedia 2017;105:194–9. https://doi.org/10.1016/j.egypro.2017.03.301.
[28] Kasaeian A, Daneshazarian R, Pourfayaz F. Comparative study of different nanofluids applied in a trough collector with glass-glass absorber tube. J Mol Liq 2017;234:315–23. https://doi.org/10.1016/j.molliq.2017.03.096.
[29] Kasaeian A, Daneshazarian R, Pourfayaz F, Babaei S, Sheikhpour M, Nakhjavani S. Evaluation of MWCNT/ethylene glycol nanofluid flow in a parabolic trough collector with glass-glass absorber tube. HFF 2019;30:176–205. https://doi.org/10.1108/HFF-11-2018-0693.
[30] Chen L, Liu J, Fang X, Zhang Z. Reduced graphene oxide dispersed nanofluids with improved photo-thermal conversion performance for direct absorption solar collectors. Sol Energy Mater Sol Cells 2017;163:125–33. https://doi.org/10.1016/j.solmat.2017.01.024.
[31] Mehrali M, Ghatkesar MK, Pecnik R. Full-spectrum volumetric solar thermal conversion via graphene/silver hybrid plasmonic nanofluids. Appl Energy 2018;224:103–15. https://doi.org/10.1016/j.apenergy.2018.04.065.
[32] Sattar A, Bofeng B, Fazal F, Farooq M, Riaz F, Hussain I, et al. Experimental investigation of photothermal performance in nanofluid-based direct absorption solar collection for solar-driven water desalination. Case Stud Therm Eng 2024;59:104464. https://doi.org/10.1016/j.csite.2024.104464.
[33] Vakili M, Yahyaei M, Ramsay J, Aghajannezhad P, Paknezhad B. Adaptive neuro-fuzzy inference system modeling to predict the performance of graphene nanoplatelets nanofluid-based direct absorption solar collector based on experimental study. Renew Energy 2021;163:807–24. https://doi.org/10.1016/j.renene.2020.08.134.
[34] Vakili M, Hosseinalipour SM, Delfani S, Khosrojerdi S, Karami M. Experimental investigation of graphene nanoplatelets nanofluid-based volumetric solar collector for domestic hot water systems. Sol Energy 2016;131:119–30. https://doi.org/10.1016/j.solener.2016.02.034.
[35] Liu J, Ye Z, Zhang L, Fang X, Zhang Z. A combined numerical and experimental study on graphene/ionic liquid nanofluid based direct absorption solar collector. Sol Energy Mater Sol Cells 2015;136:177–86. https://doi.org/10.1016/j.solmat.2015.01.013.
[36] Chakraborty S, Panigrahi PK. Stability of nanofluid: a review. Appl Therm Eng 2020;174:115259. https://doi.org/10.1016/j.applthermaleng.2020.115259.
[37] Mukherjee S, Mishra PC, Chaudhuri P. Stability of heat transfer nanofluids – a review. ChemBioEng Rev 2018;5:312–33. https://doi.org/10.1002/cben.201800008.
[38] Mehta B, Subhedar D, Panchal H, Said Z. Synthesis, stability, thermophysical properties and heat transfer applications of nanofluid – a review. J Mol Liq 2022;364:120034. https://doi.org/10.1016/j.molliq.2022.120034.
[39] Chang H, Lo CH, Tsung TT, Cho YY, Tien DC, Chen LC, et al. Temperature effect on the stability of CuO nanofluids based on measured particle distribution. Key Eng Mater 2005;295–296:51–6. https://doi.org/10.4028/www.scientific.net/KEM.295-296.51.
[40] Tavares J, Coulombe S. Dual plasma synthesis and characterization of a stable copper–ethylene glycol nanofluid. Powder Technol 2011;210:132–42. https://doi.org/10.1016/j.powtec.2011.03.006.
[41] Chen L, Xu C, Liu J, Fang X, Zhang Z. Optical absorption property and photo-thermal conversion performance of graphene oxide/water nanofluids with excellent dispersion stability. Sol Energy 2017;148:17–24. https://doi.org/10.1016/j.solener.2017.03.073.
[42] Wang X, Liu D, Liu X, He Y. Graphene oxide stabilized carbon nanotube-water nanofluids for direct absorption solar collectors. IOP Conf Ser: Mater Sci Eng 2019;556:012037. https://doi.org/10.1088/1757-899X/556/1/012037.
[43] Bepete G, Hof F, Huang K, Kampioti K, Anglaret E, Drummond C, et al. "Eau de graphene" from a KC8 graphite intercalation compound prepared by a simple mixing of graphite and molten potassium, Physica Status Solidi (RRL) – Rapid. Res Lett 2016;10:895–9. https://doi.org/10.1002/pssr.201600167.
[44] Bepete G, Anglaret E, Ortolani L, Morandi V, Huang K, Pénicaud A, et al. Surfactant-free single-layer graphene in water. Nature Chem 2017;9:347–52. https://doi.org/10.1038/nchem.2669.
[45] Bepete G, Pénicaud A, Drummond C, Anglaret E. Raman signatures of single layer graphene dispersed in degassed water, "'eau de graphene"'. J Phys Chem C 2016;120:28204–14. https://doi.org/10.1021/acs.jpcc.6b07288.
[46] Sainz-Mañas M, Caliot C, Escape C, Bataille F, Flamant G. Optical properties of a graphene nanofluid for direct absorption solar collectors. Next Materials 2025;8:100798. https://doi.org/10.1016/j.nxmate.2025.100798.
[47] Ghadimi A, Saidur R, Metselaar HSC. A review of nanofluid stability properties and characterization in stationary conditions. Int J Heat Mass Transf 2011;54:4051–68. https://doi.org/10.1016/j.ijheatmasstransfer.2011.04.014.
[48] Yılmaz Aydın D, Gürü M. Nanofluids: preparation, stability, properties, and thermal performance in terms of thermo-hydraulic, thermodynamics and thermo-economic analysis. J Therm Anal Calorim 2021. https://doi.org/10.1007/s10973-021-11092-8.
[49] Standard Tables for Reference Solar Spectral Irradiances: Direct Normal and Hemispherical on 37° Tilted Surface, (2023). doi:10.1520/G0173-23.
[50] Rioglass Solar, PTR®70 linear receiver, HCE Tubes (n.d.). https://www.rioglass.com/our-products/hce-tubes.html (accessed January 13, 2022).
[51] Babita SK, Sharma SM. Gupta, preparation and evaluation of stable nanofluids for heat transfer application: a review. Exp Therm Fluid Sci 2016;79:202–12. https://doi.org/10.1016/j.expthermflusci.2016.06.029.
[52] Ali N, Teixeira JA, Addali A. A review on nanofluids: fabrication, stability, and thermophysical properties. J Nanomater 2018;2018:6978130. https://doi.org/10.1155/2018/6978130.
[53] Celata GP, D'Annibale F, Mariani A, Sau S, Serra E, Bubbico R, et al. Experimental results of nanofluids flow effects on metal surfaces. Chem Eng Res Des 2014;92:1616–28. https://doi.org/10.1016/j.cherd.2013.12.003.
[54] Fotowat S, Askar S, Ismail M, Fartaj A. A study on corrosion effects of a water based nanofluid for enhanced thermal energy applications. Sustainable Energy Technol Assess 2017;24:39–44. https://doi.org/10.1016/j.seta.2017.02.001.
[55] Valenzuela L, López-Martín R, Zarza E. Optical and thermal performance of large-size parabolic-trough solar collectors from outdoor experiments: a test method and a case study. Energy 2014;70:456–64. https://doi.org/10.1016/j.energy.2014.04.016.
[56] Moss R, Shire S, Henshall P, Arya F, Eames P, Hyde T. Performance of evacuated flat plate solar thermal collectors. Therm Sci Eng Prog 2018;8:296–306. https://doi.org/10.1016/j.tsep.2018.09.003.